10

Fabrication of Nanomaterials by Pulsed Laser Synthesis

Khaled Habiba[1], Vladimir I. Makarov[1], Brad R. Weiner[2], Gerardo Morell[1]

[1]Institute of Functional Nanomaterials, University of Puerto Rico, San Juan, PR 00931- 3334, USA, Department of Physics, University of Puerto Rico-Rio Piedras Campus, San Juan, PR 00936- 8377, USA
[2]Institute of Functional Nanomaterials, University of Puerto Rico, San Juan, PR 00931- 3334, USA, Department of Chemistry, University of Puerto Rico-Rio Piedras Campus, San Juan, PR 00931- 3346, USA

Outline:

Introduction

The synthesis of nanoparticles has attracted considerable interest during the last decade due to their potential applications in medicine, energy and environmental remediation. However, nanoparticles were used by the ancient cultures of Egypt and Rome in amazing works of art [1-3]. Much of today's nanotechnology is focused on the systematic synthesis and characterization of new nanomaterials with enhanced properties and applications.
Pulsed Laser Synthesis (PLS) has been used to fabricate a wide range of nanomaterials, which have shown a variety of chemical, optical, magnetic, and electronic properties. PLS technique for the fabrication of materials can be traced back to the invention of the pulsed ruby laser in the mid-1960s [4]. For decades, researchers have focused on the synthesis of different materials using this technique in liquid and gas phases with solid, liquid and gaseous precursors [5-7]. There are different experimental setups for the synthesis of nanostructures using PLS, which depend on the precursor materials, the laser parameters and the ambient conditions. The appropriate selection of parameters is essential in minimizing unwanted by-products and increase the yield of the intended nanostructured materials. PLS has demonstrated excellent suitability for the synthesis of a wide range of nanoparticles in terms of the yield and size homogeneity of the produced nanomaterials. Hence, PLS has potential for the industrial manufacturing of such nanostructures.
In this chapter, the synthesis of different nanostructures by PLS and plausible mechanisms for their formation are described. In particular, an array of carbon-based nanostructures can be obtained by changing the PLS conditions and parameters. Through the application of spectroscopic and microscopy techniques, we obtained a comprehensive understanding of the nanomaterials' composition and structure.

Fundamentals of interaction of the laser beam with the matter

The interaction of the laser radiation with matter is the most important issue in the synthesis of nanomaterials with laser beams. The use of PLS for manufacturing new materials involves the appropriate selection of the laser's processing parameters with respect to the photo-physical properties of the material on which it is applied. In this section, basic concepts regarding the most common interactions of laser radiation and matter are presented.

Excitation Mechanisms of Matter Irradiated by Pulsed Laser

When the laser beam interacts with a material in vacuum, gaseous or liquid medium, the incident light can either be reflected or absorbed. The absorbed energy from the laser beam can react with the matter in a form of either a thermal or/and chemical process. Generally, the mechanisms that can possibly occur as a result of the laser- matter interactions can be categorized into two possible mechanisms. These possible mechanisms are known in the literature [8-10], as photochemical, photothermal and photophysical, are described below. For interactions between the laser and matter, the following factors should be taken into consideration:

- Physical state of the material, *i.e.* solid, liquid or gas.
- Type of the material, *i.e.* conductor, insulator, or semiconductor.

- Laser beam parameters: excitation wavelength, pulse width, laser fluence, and beam diameter.
- Impurities, defects, and crystal structure of the solid material in two interfaces experiments.
- Relaxation times of thermalization and initial excitation processes.

Photothermal Mechanism

The photothermal mechanism induced by a pulsed laser refers to the thermal activation processes inside the material, where there is a phase change due to an increase in the temperature and enthalpy of the system. The absorbed photon energy induces an excitation within the focused area of the focused pulsed laser. These types of excitations are known as the photothermal effect, thermal explosion, or pyrolytic effect, and are usually described by the relaxation times. If the relaxation time of the thermalization process (τ_T) is less than the time of initial excitation process (τ_E), *i.e.* $\tau_T << \tau_E$ then the is considered as photothermal. In some systems, this condition is not valid due to the τ_E could be longer due to the removal of some species from the surface, or structural rearrangements of atoms or molecules [8]. In the photothermal effect, the temperature jump of the spot where the laser's beam is focused is extremely high and can reach up to 10^9 K/s for nanosecond pulses and even higher for femtosecond lasers [9]. In photothermal processes the laser evaporates the material at higher laser fluence, which in turn creates heterogeneous nucleation of vapor bubbles leads to normal boiling. In this situation, rapid homogenous nucleation and expansion of vapor bubbles lead to explosive boiling or phase explosion, which carry off the solid - liquid material fragments [9, 11]. Therefore, the PLS technique can provide significant changes to the irradiated material, opening new chemical reaction pathways and reaction products, and generate novel material microstructures, nanostrcutures, phases, surface morphologies, and evaporation characteristics.

Photochemical Mechanism

The photochemical mechanism term is used for non-thermal reactions induced by photons, which are strong enough to break the bonds between molecules and generate electrons, atoms and ions. The system is described as photochemical or photolytic when the non-thermal processes are the most dominant. Laser irradiation of the matter generates large excitation in the intermediary states, which induce the photo decomposition of the chemical bonds between the molecules of the material. In that case, $\tau_T \geq \tau_E$ where the overall thermalization processes are slow and the temperature of the system remains relatively unchanged under the irradiation. In femtosecond and nanosecond pulsed lasers, direct ionization and the formation of dense electron-hole plasmas lead to direct bond-breaking, tunnel ionization, multi-photon ionization, and explosive disintegration of the lattice through electronic repulsion, which is also known as Coulomb explosion [8-9, 12-14]. This mechanism holds for the chemical reactions between excited molecules with each other or with the medium- solid surfaces, and initial processes such as photochemical desorption of species from surfaces. When both of the thermal and non-thermal processes contribute directly to the overall processing rate of the PLS system, the mechanism is known as photophysical [8-9, 15].

Approaches to the synthesis of nanomaterials

There are two major approaches in synthesizing nanomaterials: bottom-up or top-down. Depending on the experimental conditions employed, the properties and structure of the synthesized nanoparticles can be controlled. Routes for the synthesis of nanoparticles allows the control the particle size, particle geometry, doping ratio by different elements, and degree of particle agglomeration. Those particle parameters give the synthesized material new physical and chemical properties for different applications. A deep understanding of the synthetic approach is critical in order to manufacture new structures with unique properties. Many techniques have been reported regarding both approaches such as chemical vapor deposition, sol gel, PLS, sputtering, mechanical milling and other techniques. In this chapter, we are just focusing on those techniques that use pulsed laser techniques. The schematic shown in Figure 10.1 describes simply the difference between both approaches.

Bottom-Up approach

Many nanomaterials are synthesized by the interaction of atoms or/and some molecular species through a set of chemical reactions provided by the technique [16-17]. The precursor is typically a liquid or gas that is ionized, dissociated, sublimated or evaporated and then condensed to form either an amorphous or/and crystalline nanoparticle. This approach produces nanoparticles with fewer defects, homogenous chemical composition, less contamination, and particles with a narrow size distribution. In PLS technique, we can consider the infrared pulsed laser pyrolysis (IPLP), the infrared pulsed laser induced breakdown (IR-PLIB) and the Laser-induced dissociative stitching (LIDS) as three bottom-up methodology in syntheses of nanomaterials (*vide infra*).

Top-Down approach

The starting material is a bulk material of the same material to be synthesized, which is then broken into smaller and smaller fragments or particles when a source of energy is applied. The energy applied can be mechanical, chemical or thermal, or could be another form of energy such as laser irradiation. In Pulsed Laser Ablation (PLA) and Pulsed Laser Deposition (PLD), the energy is absorbed by the material and transformed into chemical and/or thermal energy to break (inter) molecular bonds of the bulk material [18-19]. This approach usually results in smaller flakes or particles with a wide size distribution, and is considered one of the disadvantages of the top-down method. It is possible to overcome that disadvantage and synthesize nanoparticles of precise size using a focused ion beam or lithography, but it requires expensive equipment [20]. For this reason, the bottom- up approach is considered simpler and more precise in the synthesis of small nanoparticles less than 100 nm, and the top-down approach is preferred for the synthesis of thin films and nanoparticles larger than 100 nm.

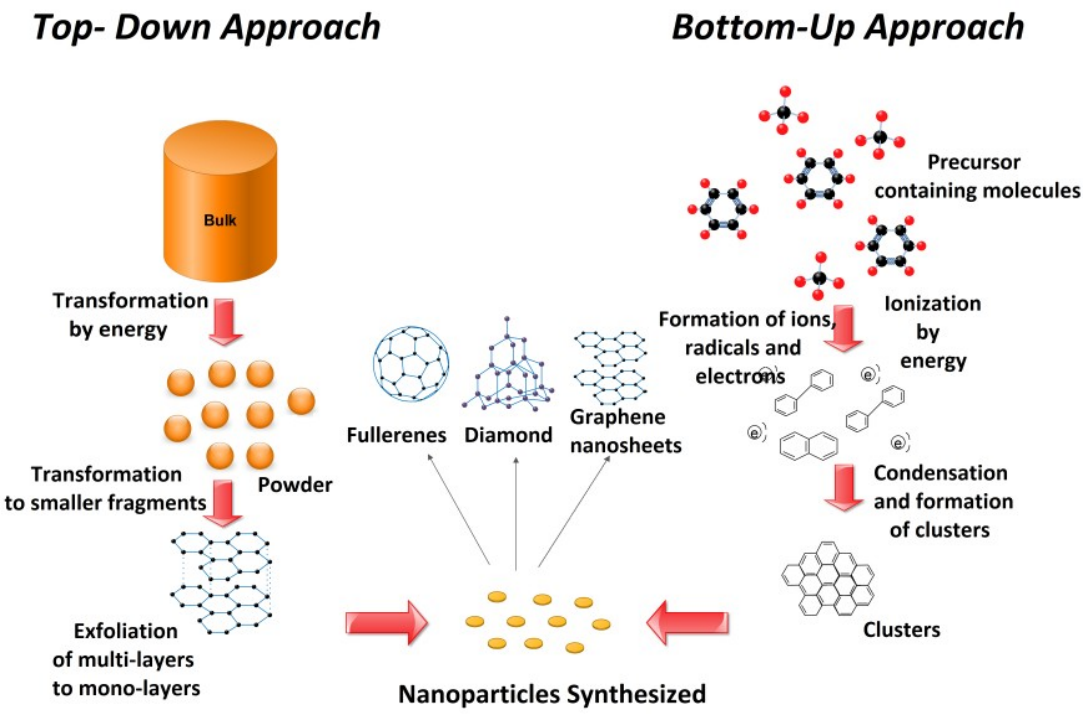

FIGURE 10.1
Bottom-up and the top-down approaches in synthesis of carbon-based nanomaterials

Types of PLS

PLS is a powerful, flexible and versatile technique in the synthesis of many nanoparticles without employing special external conditions, such as high pressure or high temperature. PLS is flexible in that it can be integrated with other techniques such as chemical vapor deposition [21]. In addition, it can be used to synthesize various nanostructures via different experimental setups (see Figure 10.2), or it can be used to fabricate the same nanostructures by different approaches, making it a versatile technique. In this section, some of the different nanostructures synthesized by different PLS experimental schemes methods reported in literature will be discussed.

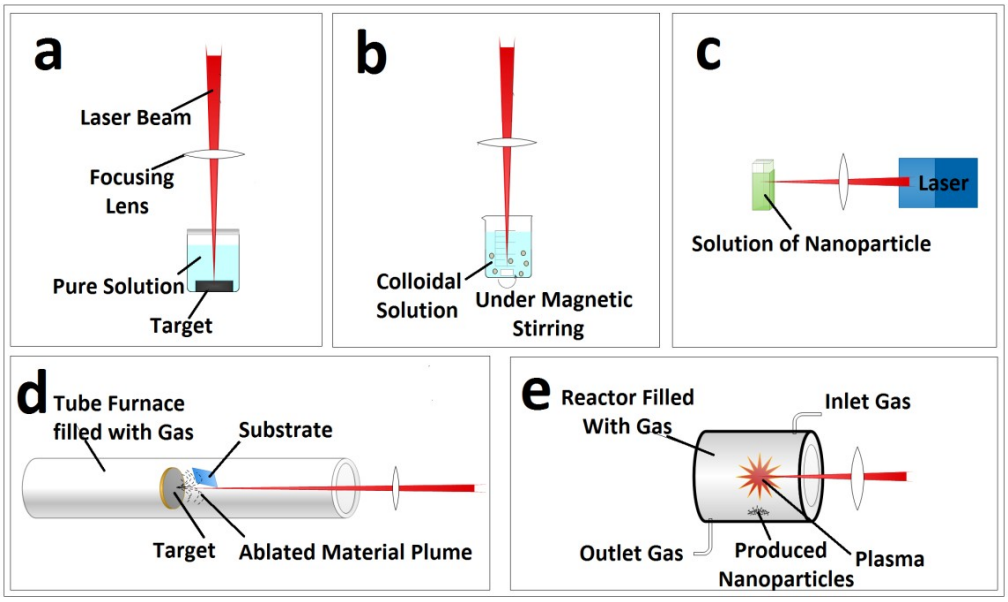

FIGURE 10.2
Experimental configurations in PLS systems where a focused beam irradiates,: a) a solid target placed in a pure solution; b) a colloidal solution; c) a solution of nanoparticles is irradiated by a focused beam; d) a solid target placed inside a tube furnace with a nearby substrate to collect the material deposition; and e) a reactor filled with a gaseous precursor

Synthesis of nanoparticles by PLA

PLA is used in the top-down synthesis of nanomaterials, such as nanotubes [22], nanowires [23], nano-ribbons [24], quantum dots [25-27], and even nano-flakes of the material [28]. The technique is widely used by many researchers in the synthesis of both inorganic and carbon-based materials with varying particle sizes and in high yield. PLA was first reported by Patil *et al.* in 1987[29], forming iron oxides with metastable phases by PLA of a pure iron target placed in water. Since then, many researchers have developed syntheses by liquid phase pulsed laser ablation (LP-PLA) and gas phase pulsed laser ablation (GP-PLA). The laser beam of a specific wavelength is focused by a lens through a transparent window of the reactor containing gas-solid or liquid -solid interfaces. When the laser beam impinges upon the surface of a solid target (*i.e.* bulk or powder), the light interacts with the matter and generates a plume of nanoparticles of the target material, which subsequently react with the gas or liquid. It is possible to dope the synthesized material by choosing a precursor containing the dopant element as a reactant during the laser irradiation [30].

Synthesis of nanoparticles by GP-PLA

A focused laser beam ablates a solid target located inside a chamber filled with a pure gas or a mixture of inert gases. The role of the gas in this type of PLA is simply to control the plasma expansion, and the plasma plume dynamics [31-32]. At low laser power, the beam heats the surface of the target resulting in evaporation. This experimental setup is sometimes used in conjunction with an additional catalyst or applied external temperature to produce nanomaterials, such as in the case of carbon nanotubes (CNT)

[33]. At higher laser powers, plasma is created in that gaseous condition, and the high temperature required for the synthesis of some nanomaterials could be achieved without the need of an external high temperature source [34]. The GP-PLA is also known as laser chemical vapor deposition LCVD, in which the gas is working as a precursor.

Synthesis of nanoparticles by LP-PLA

In LP-PLA, the solid target is immersed in a liquid medium inside the reactor and irradiated by a focused laser beam. The beam hits the surface of the solid target, vaporizes it, and forms an ablation plume, which contains atoms, ions, molecules, clusters and particles. The intermediate reactive products in the plume react with the molecules of the surrounding liquid, producing nanostructures containing atoms from both the original target and the liquid. The confinement built by the liquid layer in combination with the high temperature and high pressure induced by the focused pulsed beam offers an ideal condition for the formation of metastable phases, favors the synthesis of various nanostructures [35]. The choice of the liquid, the solid target, laser wavelength, and the laser power are the keys to successfully synthesizing nanostructured materials of specific size and properties. This method is simple and versatile and does not require an expensive setup compared to other techniques *i.e.* chemical vapor deposition (CVD). The nanomaterials synthesized by this method are usually a colloidal suspension, or a homogenous mixture of soluble nanoparticles, and can be collected by filtration or evaporation.

Synthesis of nanoparticles by IPLP

The synthesis of nanomaterials can be achieved by irradiation of a gaseous hydrocarbon by a focused infrared pulsed laser beam. This method is typically used to synthesize organic molecules and carbon-based nanoparticles, where the irradiation of gas phase precursors allows for a pyrolysis effect, similar to other techniques, *e.g.* arc discharge [36-37]. Gas mixtures consist of three components: photosensitizers, buffer gas, and precursor gas. The photosensitizer absorbs the laser radiation and reacts via collisions with the precursor gas. The buffer gas is typically an inert gas such as He or Ar, and serves as a carrier or quencher for the products of the reaction. The photosensitizer/ precursor flow ratio, the laser power, the selection of gas precursors, and the time of irradiation are critical parameters to optimize the synthesis of different carbon nanostructures. Moreover, aromatic hydrocarbons in the gas phase can also be used as a precursors, as reported by Llamas-Jansa and co-workers [36]. They have used benzene in the synthesis of conductive graphitic structures and fullerene-like nanomaterials with energy gaps of 0.8-1.5 eV. Laser pyrolysis can also be initiated by a continuous wave laser to synthesize similar carbon nanostructures [38].

Synthesis of nanoparticles by IR-PLIB

A focused pulsed infrared laser is used to irradiate a liquid hydrocarbon. The focused laser generates a strong electric field which induces the ionization of the hydrocarbon. In the ionization region, the intense field accelerates the free electrons which in turn collide with hydrocarbon molecules, and eject more electrons. This phenomenon is known as avalanche multiplication of free electrons and induces the breakdown of the liquid hydrocarbon [13]. The photo-decomposition of the liquid precursors most likely proceeds via a photothermal mechanism. Toyota and co-workers have used a nanosecond infrared pulsed Nd:YAG laser to irradiate aromatic hydrocarbon such as toluene and benzene [39],

leading to the production of amorphous carbon and higher order aromatics, such as anthracene and phenanthrene.

Synthesis of nanoparticles by LIDS

The synthesis of carbon nanostructures, employs a halogen containing aromatic compound at room temperature, which is irradiated by a UV laser. The UV pulsed laser induces the photo-cleavage of the carbon-halogen bond, which is followed by stitching' the photo- generated free radicals into functional nanostructured forms of carbon. This method is also known as Pulsed Laser-induced Photochemical Stitching (PLPS) and was first reported by Gokhale *et al.* [40]. Using the same mechanism proposed by Gokhale *et al.*, carbon nano-spheres were synthesized by the laser irradiation of halogenated hydrocarbons [41].

Synthesis of nanoparticles by Pulsed Laser Photolysis (PLP)

PLP consists of irradiating a liquid colloidal suspension by UV or IR pulsed laser usually at room temperature. The method has been used for the synthesis of both organic and carbon based materials [28], and inorganic nanoparticles [42-44]. Nkosi *et al.* reported the synthesis of FePt nanoparticles by the irradiation of a solution of iron acetylacetonate and platinum acetylacetonate. They have succeeded in controlling the size and the ratio of the metals by changing the laser energy [42]. The mechanism of formation of these nanostructures using this method is not clearly understood, however, the authors have proposed a photochemical reaction.

Synthesis of nanoparticles by PLD

PLD is one of the most common and versatile methods in the synthesis of thin films of complex-oxide hetero-structures [45-46], semiconductors [47-50], and ceramics [51-56]. A high-power laser is used to vaporize a bulk target placed on a holder congruently onto a substrate placed close to the target inside the vacuum chamber. A set of optical components is used to focus the laser beam over the target surface. The chamber typically is at high vacuum, or it can be filled at low pressure with a background gas such as oxygen for deposition of oxides. The operating temperature can be varied from room temperature to high temperature, depending on the experimental procedures. When the laser beam hits the surface of the target in vacuum, it generates the plasma plume containing neutrals and ions. The plume carrying the ablated material is deposited on the surface of the substrate, which is located parallel to the target [57-58].

Synthesis of different nanomaterials

Major approaches in the synthesis of nanomaterials are presented, and a review of the synthesis of various organic and inorganic nanostructures by PLS has been carried. We will focus in this chapter on the synthesis of new nanostructures such as boron nitride and graphene using novel methods in the PLS technique.

Synthesis of inorganic nanomaterials by PLS

The synthesis of inorganic nanomaterials has attracted the attention in the last decade due to their high surface area, and the surface plasmon resonance [59-60]. The revolution in solid state physics and the need of magnetic, superconductor and semiconductor compounds has provided the motivation to focus on synthesis of inorganic materials. Since some metals are good magnetic materials and silicon is presently the most common semiconductor, it follows that the synthesis of inorganic materials using PLS has increased. Herein, we are going to present some examples on the synthesis of nanoparticles using this technique.

Synthesis of different metallic nanoparticles by PLS

The synthesis of metal nanoparticles, such as gold, platinum, silver and palladium have been studied extensively, since they have a wide applicability [61-63]. LP-PLA is widely used in synthesis of metal colloidal suspension of nanoparticles of metals with a size range from a few nanometers up to hundreds of nanometers [64]. This method is considered as a green method since it does not require the use of highly toxic chemical reactants [65]. The variation of the chemical properties of the surrounding liquid used during the laser irradiation can control both the size of the synthesized nanoparticles and their stability [66-68], and it was found that the energy of the laser pulse used will also add control to the particle size distribution [69]. Kubiliute *et al.* reported a change in the shape of the gold nanoparticles synthesized by LP-PLA [70]. They have shown that their synthesized gold nanoparticles change in shape from spherical to elliptical when a second laser irradiates the colloidal suspension of the spherical gold nanoparticles produced from the first irradiation. Similarly, the synthesis of metal oxides [71], and quantum dots [26-27] have been reported. Table 10.1 summarizes different methodology for the synthesis of different inorganic nanostructures using PLS.

TABLE 10.1
Examples of synthesis of inorganic nanomaterials using different methods of PLS

Target Used	Method	Nanostructured Synthesized	References
Gold metal plate immersed in aqueous solution of sodium dodecyl sulfate	LP-PLA	Gold nanoparticles	Mafuné *et al.* (2002) [61]
Silver plate immersed in different organic solutions	LP-PLA	Silver nanoparticles	Amendola *et al.* (2007) [62]
Si-Fe Target	GP-PLA integrated with a tube furnace	Silicon Nanowires	Fukata *et al.* (2005) [23] Morales *et al.* (1998) [63]
GaAs target immersed in deionized water or ethanol	LP-PLA	GaAs nanocrystals	Salminen *et al.* (2012) [72]
CdSe bulk target immersed in methanol	LP-PLA	CdSe nanoparticles	Semaltianos *et al.* (2008) [27]
Metal target of Ni, Co, and Ni50Co50 in ethylene Glycol	LP-PLA	Nanoparticles of Ni, NiCo, and pure Co	Zhang *et al.* (2008) [73]
Bulk Palladium immersed in water, acetone or ethanol	LP-PLA	Nanoparticles of Palladium or palladium hydride	Semaltianos *et al.* (2013) [74]
Bulk target of titanium oxide immersed in deionized water	LP-PLA	Nanoparticles of titanium oxide	Nath *et al.* (2011) [75]
Polycrystalline MoS2 target made from pressing powder of MoS2 immersed in water and n-decane	LP-PLA	Inorganic fullerene-like MoS2 nanostructures	Compagninia *et al.* (2012) [76]

Synthesis of Boron Nitride nanostructures using PLS

The synthesis of boron nitride (BN) nanostructures has attracted much attention in materials science due to its applications and numerous properties, *i.e.* good thermal conductivity, hardness, low thermal expansion, high electrical resistance, good thermal shock resistance and chemical inertness [77–81,52-56]. Moreover, much research has been focused on the synthesis of various forms of BN, such as boron nitride nanotubes (BNT), cubic boron nitride (c-BN), and hexagonal boron nitride (h-BN).
We will focus here on the synthesis and the characterization of c-BN and h-BN, which are two promising forms of BN. There are numerous reports on the synthesis of BN nanostructures using many

techniques [51-57, 82-83]. Table 10.2, summarizes the variations of PLS used for different forms of BN using different experimental setups.

TABLE 10.2
Synthesis of boron nanostructures using different methods of PLS

Target used	Method	BN Nanostructure Synthesized	References
▪ **h-BN in aceton**	LP-PLA	Nanofibers	Nistor *et al.* 2010 [57]
▪ **h-BN in aceton**	LP-PLA	Nanotubes	Nistor *et al.* 2010 [57]
▪ **BN**	Plasma-assisted PLD	Nanocapsules	Komatsu *et al.* 2002 [56]
▪ **h-BN**	PLD	Nanosheets	Sajjad *et al.* 2013 [53]
▪ **BN**	PLD	Nanorods	Sajjad *et al.* 2011 [52]
▪ **h-BN**	PLD	Thin Films	Sajjad *et al.* 2011 [54]
▪ **h-BN**	Ion assisted PLD		Reisse *et al.* 1999 [55]

Recently, we have developed a novel method of the synthesis of high yields of c-BN and h-BN nanostructures using PLS in the gas phase [51]. This method has produced particles of BN with sizes in range of 20–100 nm and a ratio of B/N=1. When compared to the other methods reported in the literature, this methodology has solved some common problems previously encountered *i.e.*, low yields, inability to control the stoichiometry of B and N, and high levels of impurities.

A small reactor with a quartz window was flushed with nitrogen and evacuated to high vacuum (10^{-6} Torr), and then filled with 40 mbar of borazine vapor. A focused pulsed (10Hz) Nd:YAG laser beam containing both the fundamental (1064 nm) and the first harmonic (532 nm) was employed to irradiate the borazine vapor inside the reactor for 60 min. A powder of the synthesized BN was collected on the surface of a substrate placed inside the reactor.

The resulting BN nanostructures were characterized using Raman spectroscopy, Fourier transform infra- red spectroscopy (FTIR), Scanning Electron Microscopy (SEM), Transmission Electron Microscopy (TEM), and X-ray Diffraction (XRD). The SEM image in Figure 10.3a reveals porous nanostructures of BN covering the surface of a silicon substrate. The TEM was employed to show the size range of the synthesized nanoparticles. The TEM images (Figure 10.3b-c) shows nano-crystals with sizes in the range of 20 -100 nm.

Raman spectroscopy is a standard technique used in material science for the characterization of nanostructures by observing fingerprints, characteristic of those structures from the obtained spectrum. The Raman spectrum in Figure 10.4a shows two sharp peaks at 805 cm^{-1} and 1367 cm^{-1}, and two broad bands at *ca.* 1000 cm^{-1} and *ca.*1400 cm^{-1}. The sharp peaks correspond to the h-BN and are consistent with the h- BN synthesized by other methods [51]. The two broad bands were assigned to c-BN, as reported by Reich *et al.* [84]. This indicates that c-BN and h-BN were probably synthesized simultaneously. The Raman spectrum is consistent with the TEM images which show some cubic structures as well as some flakes corresponding to c-BN and h-BN, respectively.

FTIR spectroscopy was employed to characterize the synthesized BN nanostructures as a complimentary technique. The FTIR spectrum in Figure 10.4b shows three bands at 802.23, 1068, and 1367.19 cm^{-1}. It is found that the bands at 802.23 and 1367.19 cm^{-1} corresponds to h-BN, and the band 1068 cm^{-1}, interestingly, corresponds to c-BN [85-88].

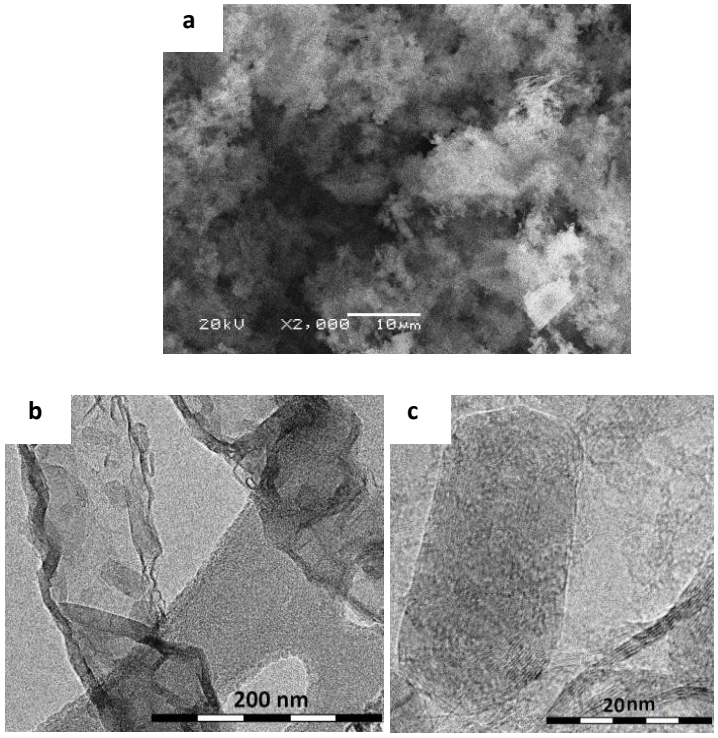

FIGURE 10.3
Characterization of the nanoparticles under microscopy showing: (a) SEM images of BN nanostructures; (b) TEM image of BN nanostructures with sizes in the 20 to 100 nm range. (c) TEM image of the synthesized cubic BN nanostructures. Copyright © 2013. Reproduced with permission from Hindawi Publishing Corporation

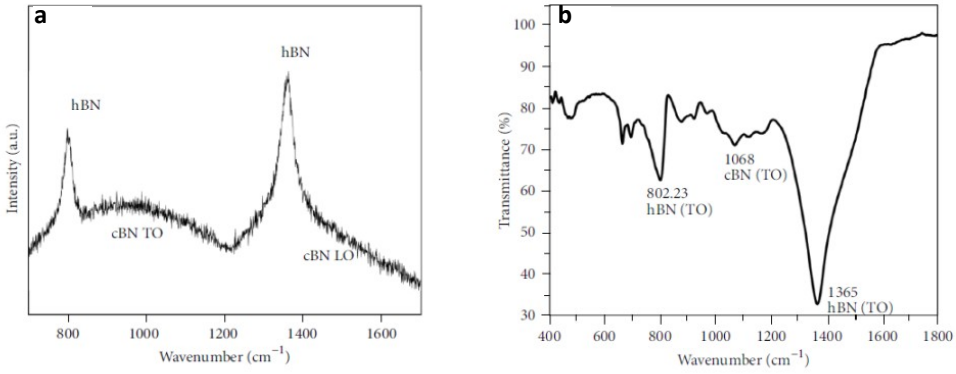

FIGURE 10.4
(a) Raman spectrum consists of two characteristic bands at 803 and 1356 cm^{-1}, which correspond to hexagonal BN; (b) The FTIR consists of the bands at 802.23 and 1367.19 cm^{-1} related to h-BN nanostructured materials, and the absorption band at 1068 cm^{-1} related to c-BN nanostructured materials [51]. Copyright © 2013. Reproduced with permission from Hindawi Publishing Corporation

The XRD technique can be used to identify the crystalline structure for materials in powder form. The diffractogram in Figure 10.7 shows the planes (002), (100), and (104) for h-BN. The plane (004) corresponds to the c-BN [51]. The peak at 39° for the plane (111) corresponds to Pt, to which the BN powder was mounted. These data confirm the data obtained by microscopy, FTIR, and Raman.

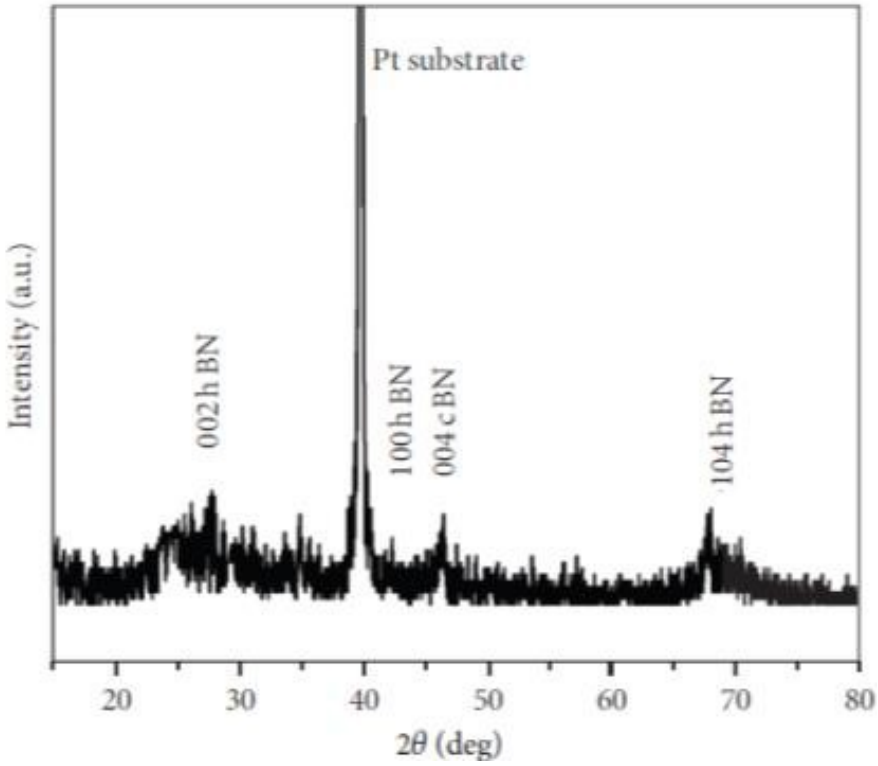

FIGURE 10.5
X-ray diffractogram reveals the (002), (100), and (104) peaks, which corresponds to h-BN material, and the (004) peak corresponds to c-BN [51]. Copyright © 2013. Reproduced with permission from Hindawi Publishing Corporation

It was possible to synthesize h-BN and c-BN nanostructures using PLS, and the particles synthesized were in the range of 20-100 nm. The method has demonstrated a new simple, efficient, and versatile technique in the synthesis of BN nanostructured materials. The method is cost effective compared to other techniques using more expensive equipment, and produces high yields up to 83% by weight.

Synthesis of Organic and carbon-based Nanomaterials by PLS

Carbon-based materials can be defined as organic materials, *i.e.* polymers, lipids, sugars, proteins, and different allotropes of carbon such as, graphite, fullerenes, diamond, carbon nanotubes, and amorphous carbon. During the last ten years and in particular, after the rise of graphene [89], thousands of reports in the literature have been directed to the synthesis and study of such carbon-based materials due to their unique chemical and physical properties [90-92]. Graphene is a promising material for numerous applications [93-95], and an excellent candidate for the fabrication of electronic

devices replacing silicon. In addition to graphene, much interest was dedicated recently to polymers and other organic materials in different fields, *i.e.* the fabrication of organic photovoltaic cells [96-97], and biomedical applications [98-100]. The motivation for using organic materials for those applications is found to be that they are biodegradable, greener, and much less toxic than inorganic materials used in similar applications. Many advances in this area have involved the synthesis of different carbon-based nanostructures using various methods, *i.e.* CVD [101-104], thermal exfoliation [105], electrochemical synthesis [106], *in-situ* polymerization [107], and PLS [22,25,108-118]. In this section, we focus only on the synthesis of organic nanomaterials using PLS, and in particular, on our recent published report on the synthesis of graphene quantum dots (GQDs) by PLS. Table 10.3. summarizes different experimental methods used to synthesize different carbon nanostructures using PLS.

TABLE 10.3
Synthesis of carbon-based nanomaterials using different methods of PLS

Precursor/ Target used	Method	Carbon Nanostructured Synthesized	References
▪ **Metallic target in Ethanol.**	LP-PLA	CNT	Chen *et al* 2005 [22]
▪ **Target of Nickel-cobalt-Graphite.**	Pulsed Laser Vaporization		Schauerman *et al.* 2009 [109]
▪ **Graphite target in de-ionized water.**	LP-PLA LP-PLA		Yang *et al.* 2007 [112]
▪ **Graphite target in de-ionized water.**		Diamond	Amans *et al.* 2009 [113]
▪ **Graphite target placed inside liquid nitrogen.**	LP-PLA	Graphene	Mortazavi *et al.* [117]
▪ **Benzene- Nickel oxide suspension.**	PLP		Habiba *et al.* 2013 [108]
▪ **Highly oriented pyrolytic graphite in water.**	LP-PLA	GQDs	Russo *et al.* 2013 [25]
▪ **Carbon target inside chamber filled of water vapor and Argon.**	GP-PLA	Carbon Dots	Sun *et al.* 2006 [115]
▪ **Carbon powder dispersed in different solvents.**	LP-PLA		Li *et al.* 2010 [116]
▪ **Graphite powder dispersed in acetonitrile.**	LP-PLA	Polyyenes	Wakabayashi *et al.* 2012 [110]

▪ **Graphite rod inside chamber filled with Argon**	GP-PLA	Fullerenes	Oyama *et al.* 1997 [118]
▪ **Silicon substrate covered with amorphous and placed inside an aqueous solution of water, ethanol, acetone and low concentration of inorganic salts solution.**	LP-PLA	Micro and Nano-cubes of Carbon	Liu *et al.* 2008 [114]
▪ **Carbon black powder in de- ionized water.**	LP-PLA	Carbon onions	Hu *et al.* 2009 [111]

Synthesis of GQDs

GQDs are small, planar nano flakes of graphene in the size range of 2-20 nm across, a few atomic layers thick, resulting in a high surface-to-volume ratio. GQDs have received considerable attention due to their unique properties, such as: size and excitation dependent photoluminescence (PL), unique physical and chemical properties, combined with resistance to photobleaching, biocompatibility and low toxicity. Furthermore, GQDs have demonstrated a wide range of promising applications in bioimaging [108,119-120], drug delivery [121], photodynamic therapy [122], and photocatalysis [123]. They may also have additional uses in photonics [124] photovoltaic cells [125], and electronic [126] devices.

The synthesis of these unique graphene nanostructures presents various challenges to researchers, namely to provide a simple method for the production of good quality GQDs at high yield and narrow size distributions. There are numerous reports on the synthesis of GQDs using the top-down approach [25,119-120,128], and only a few groups have reported their synthesis using the bottom-up approach [41,108,127]. Recently, we reported a new method for the synthesis of intrinsically luminescent GQDs by PLS [108]. In this section, we will discuss briefly the recent developments in our laboratory related to the synthesis of GQDs.

We have prepared a mixture of 0.255 wt.% nickel (II) oxide powder (NiO) in 99.745 wt.% benzene, which was then irradiated for 30 min with a 1064 nm pulsed Nd:YAG laser (Continuum Surelite, 10 Hz, 10 ns pulse width). The laser power density was adjusted to 15.9 x 10^8 W cm^{-2}, corresponding to a laser energy of about 30 mJ/ pulse. The resulting mixture of GQDs, nickel oxide (NiO) and benzene was centrifuged at 5000 rpm for 15 min, leaving the GQDs in the supernatant, while the nickel oxide particles remained in the pellet. The GQDs were then separated from the benzene by rotary evaporation, and dissolved in deionized water. The aqueous solution of the GQDs was centrifuged at 10,000 rpm, and finally, filtered using syringe filters to get a homogenous aqueous solution of GQDs. After irradiation of the benzene- nickel oxide mixture by the pulsed laser, we observed a change in the color of the suspension from clear to yellowish with some black particles suspended. After a few hours, the black particles settle to the bottom and leave the yellowish solution as a supernatant. The black precipitate and the yellowish solution were characterized separately following separation, by microscopy and spectroscopy techniques.

When the yellowish solution was separated from benzene, the material remained after the separation was dissolved then in deionized water. When the solution of the carbon structure synthesized was subjected to a UV lamp, we observed a blue luminescence from the solution (see Figure 10.6).
The luminescence motivated us to further explore the synthesized carbon structure. We employed high-resolution Transmission Electron Microscopy (HR-TEM) to examine the structure of the filtered particles. The HR-TEM images in Figure 10.7 shows some nanostructures in the range of 2- 6 nm with a hexagonal crystalline structure. In Figure 10.7c the lattice spacing was measured and found to be 0.213 nm, which corresponds to the {1100} lattice fringes of graphene [128-129].

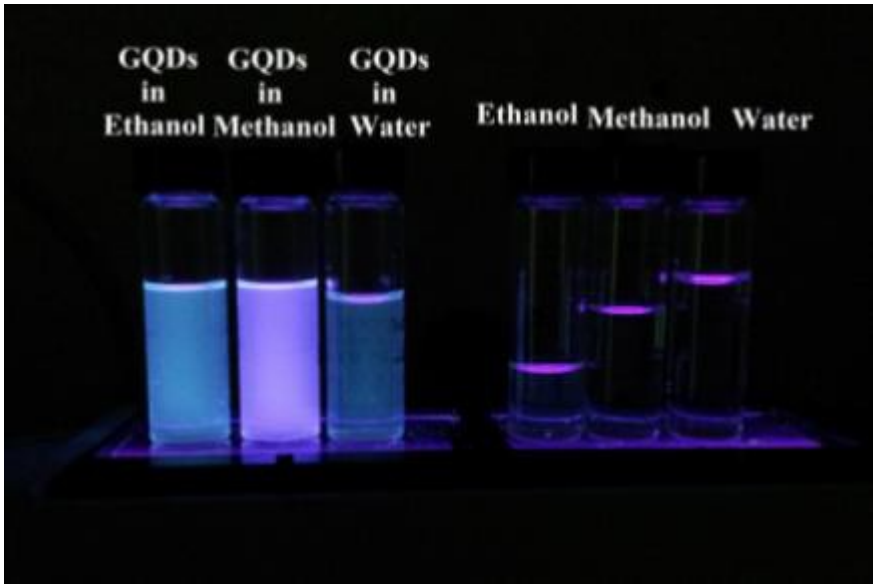

FIGURE 10.6
GQDs show strong luminescence to the naked eye under UV light [108]. Copyright © 2013. Reproduced with permission from Elsevier

To verify the chemical composition of the synthesized nanostructures, we applied Electron Energy Loss Spectroscopy (EELS) as a complimentary technique. EELS measurements shown in Figure 10.8 are dominated by the carbon edge region that shows 1s–p* transition of sp^2 bonded carbon at 285 eV, and the 1s–σ* transition of sp^3 bonded carbon at 292 eV. When the EELS data for the synthesized carbon nanostructures in our experiments were compared with the data obtained for GQDs synthesized by other methods, we found a high level of correspondence and concluded that our carbon nanostructures were GQDs [127-128].

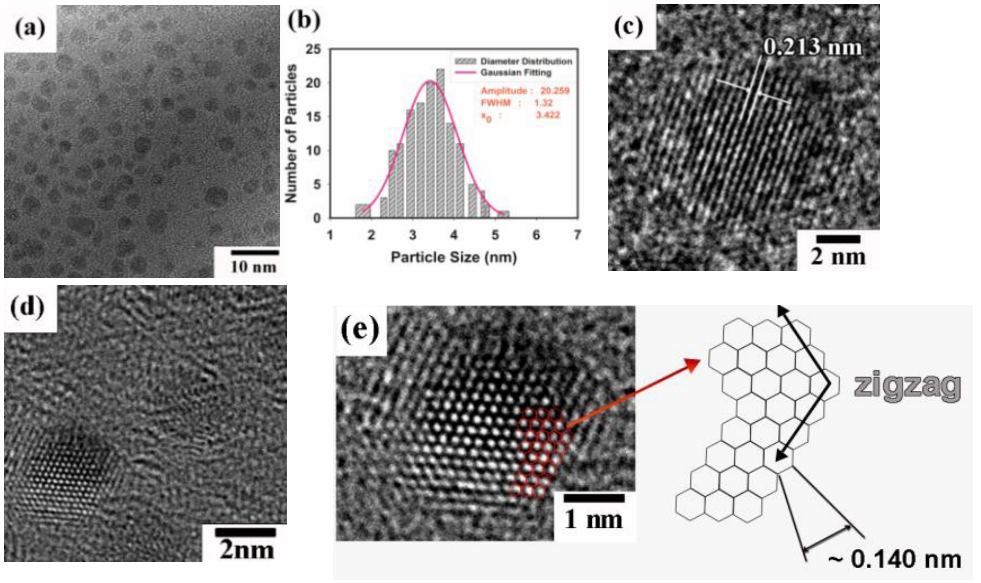

FIGURE 10.7
Characterization of the nanoparticles under HR-TEM showing: (a) the abundance and size range of the nanoparticles; (b) the statistical distribution of particle size peaking at 3.4 nm; (c) the measured lattice parameter of 0.213 nm corresponding to the (1100) in-plane lattice fringes of graphene;
(d) the fast Fourier transform (FFT) analysis corresponding to the lattice fringes of graphene; and (e) the zigzag structure of the particles' edges consistent with grapheme [108]. Copyright © 2013. Reproduced with permission from Elsevier

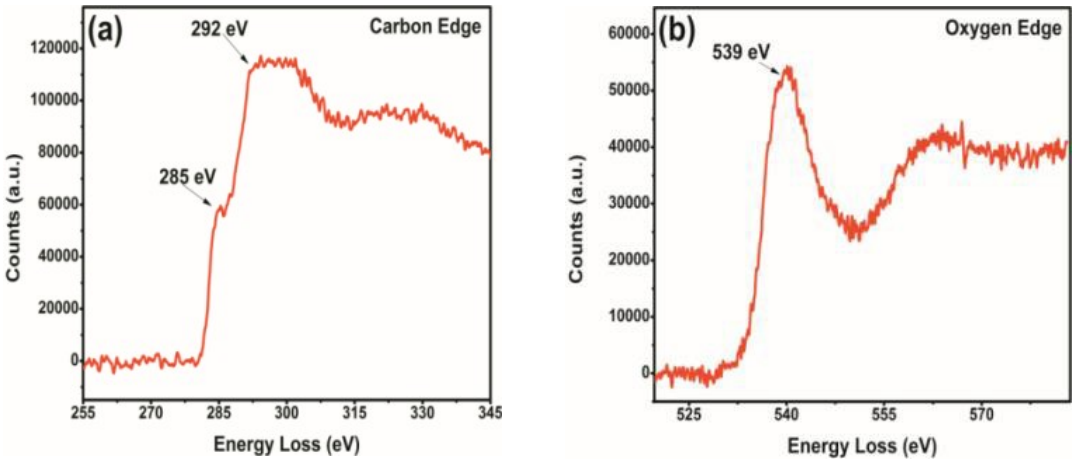

FIGURE 10.8
EELS spectra of the nanoparticles showing: (a) a prominent carbon edge around 292 eV, and
(b) a weak oxygen edge around 539 eV [108]. Copyright © 2013. Reproduced with permission from Elsevier

The Raman spectrum in Figure 10.11 shows the D-band at 1352 cm^{-1} arising from the disorder in sp^2 hybridized carbon, and the G-band at 1594 cm^{-1} corresponding to graphitic structures. The broad bands centered at 2670 cm^{-1} and 2929 cm^{-1} correspond to the 2D and D + G bands, respectively [130].

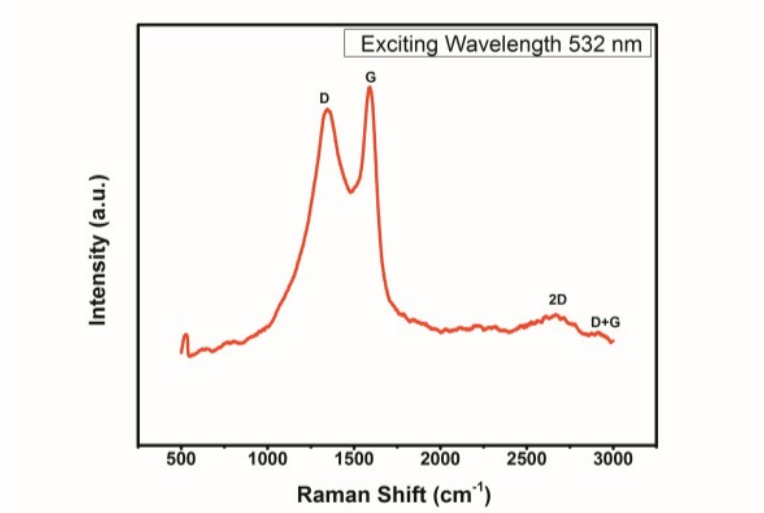

FIGURE 10.9
Raman spectrum of GQDs showing the D-band at 1352 cm^{-1}, G-band at 1594 cm^{-1}, and 2D band centered around 2670 cm^{-1} [108]. Copyright © 2013. Reproduced with permission from Elsevier

The above- analyses in addition to the other experiments reported in the article [108], indicate that the fluorescent GQDs nanoparticles fabricated by PLS are indistinguishable from the GQDs synthesized by other methods reported [25,119-128]. Therefore in this context, the analyses of the mechanism of formation of GQDs by the pulsed laser technique has been described.

Proposed mechanism of GQDs synthesis by PLS

When the pulsed laser beam is focused inside the mixture of benzene and the nickel oxide catalyst, GQDs are formed. Our hypothesis for the production of GQDs is that they result the superposition of two mechanisms: (*i*) laser-induced thermalization of the nickel oxide suspended in benzene; and (*ii*) laser-induced electron-tunneling ionization, resulting from the strong electric field induced by the pulsed laser radiation (see Figure 10.10). The second mechanism would occur as a result of the first mechanism, in which the electrons generated will then induce the electron-tunneling ionization. This effect is induced when the electric component of the laser radiation accelerates the electrons produced in the first mechanism, which in turn produces a plasma. The plasma expansion subsequently induces the breakdown of benzene, leading to the formation of some radicals, which will interact with the active centers of the catalyst. Along these same lines, Wesolowski *et al.* reported a mechanism for the formation of carbon nanostructures via the pulsed laser irradiation of a ferrocene/benzene solution [28]. Their mechanism is similar to our hypothesis, where the authors showed ionization followed by dissociation of ferrocene.
Since the nickel oxide particles absorb the laser energy as black-bodies to produce the catalytic active centers. Following this hypothesis, it was observed that the particles of the catalyst change their sizes and shape after irradiation by using the Field Emission SEM (FE-SEM) microscopy. The image in Figure

10.11a shows the particles of the nickel oxide after it was suspended in benzene and deposited on a silicon substrate (before irradiation). We observe that they agglomerate and they form micrometer-size clusters (Figure 10.10). Figure 10.11b shows that the nickel oxide nanoparticles have undergone a reduction in size to a few hundreds nanometers and are spherical in shape after irradiation. This result is consistent with an increase in the absorption cross section of these particles as their size increases, *i.e.* a blackbody. Moreover, we propose that the laser pulse duration time (τ_p) is much shorter than the space expansion time (τ_{exp}) of the heated particles of the nickel oxide suspended in the benzene. The characteristic time (τ_T) of the thermalization of benzene is also much longer than (τ_p), where $\tau_p << \tau_{exp}$ and $\tau_p << \tau_T$. Since the absorbed laser radiation energy is sufficient to evaporate and/or fragment the nickel oxide particles we expect and observe that the catalyst particles change their size and shape after irradiation. The presence of porous structures surrounding the nickel oxide particles which we found to be graphene nanoparticles [108]. The formation of these carbon nanostructures indirectly confirms the second mechanism, in which secondary processes break down benzene into smaller fragments. These radicals interact with the active centers resulting from the first mechanism to produce graphene nanostructures.

Based on our hypothesis, it would follow that other blackbody absorbers would produce the same results. To test this, we have used silver particles as a catalyst and under the same laser parameters and experimental conditions. Figure 10.12 shows the silver catalyst produce similar results to nickel oxide following irradiation the benzene mixture. Figure 10.12a shows the silver powder before irradiation, we observed that they agglomerate and form micrometer-size clusters as described in the mechanism. The image shown in Figure 10.12b reveals the formation of graphene-like nanostructures surrounding the silver nanoparticles. Note that the size range of the silver nanoparticles is less than 100 nm after irradiation. We applied the same characterizations techniques to characterize the synthesized carbon nanostructures using silver, as we did for the nickel oxide catalyst. The carbon material was filtered from the silver nanoparticles. We employed the HR-TEM technique for the synthesized particles. The HR-TEM images in Figure 10.13 correspond to the synthesized GQDs by using the silver as a catalyst. Figure 10.13a shows the formation of the GQDs at high density and with a narrow size distribution of 1-3 nm (see Figure 10.13b). To verify that the synthesized carbon nanostructures are graphene nanoflakes and GQDs, we employed Raman spectroscopy. The Raman spectrum (Figure 10.14) of the carbon nanostructures synthesized using silver as catalyst is similar to that of GQDs and porous graphene from both our laboratory and other research groups [25,108,131]. These experimental results are consistent with the proposed mechanism described above.

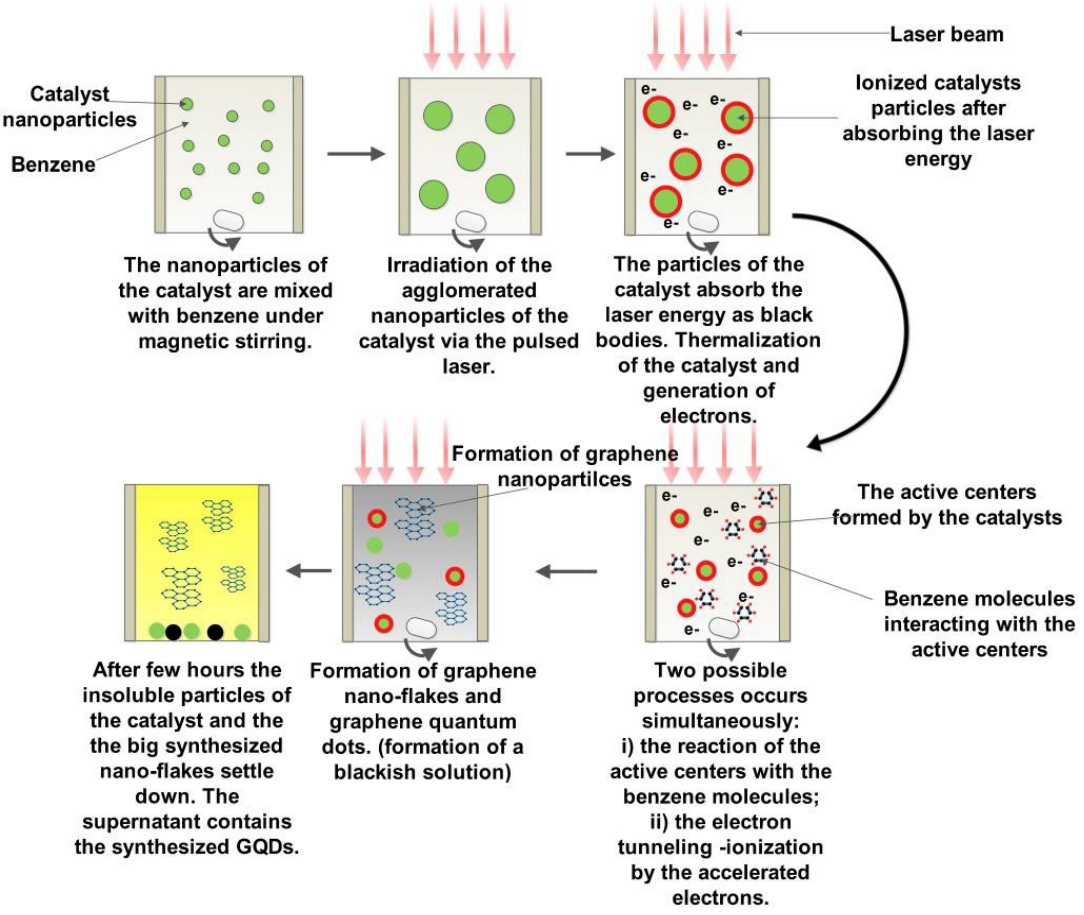

FIGURE 10.10
Proposed mechanism for the synthesis of GQDs by PLS, in which the agglomerated catalyst nanoparticles are irradiated in benzene. The particles undergo ionization and dissociation, while benzene undergoes breakdown leading to the formation of hydrocarbon radicals. The radicals react with the catalyst nanoparticles resulting in the synthesis of GQDs

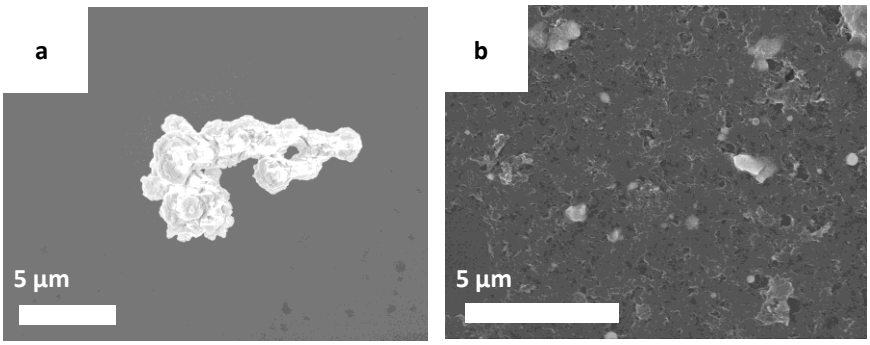

FIGURE 10.11
Characterization of catalysts and materials synthesized before and after the laser irradiation using the FE-SEM microscopy: (a) Image of the nickel oxide powder before irradiation; (b) Image of the porous graphene synthesized and the nickel oxide nanoparticles after the laser irradiation

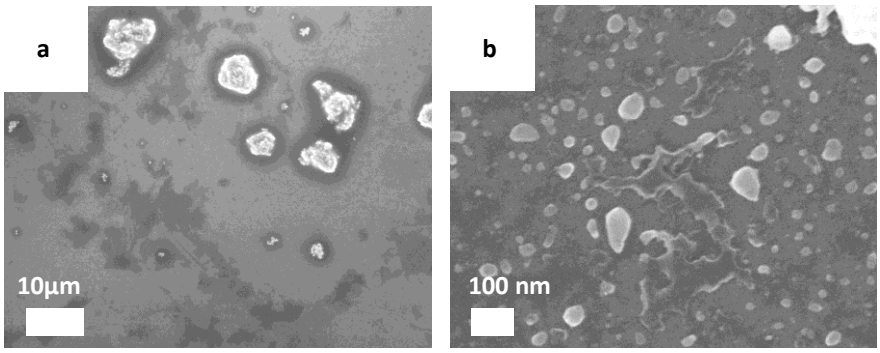

FIGURE 10.12
Characterization of catalysts and materials synthesized before and after the laser irradiation using the FE-SEM microscopy: (a) Image of the silver powder before irradiation, the silver agglomerate and forms micrometer –size clusters; (b) Image of the graphene nanostructures synthesized and the silver nanoparticles after the laser irradiation

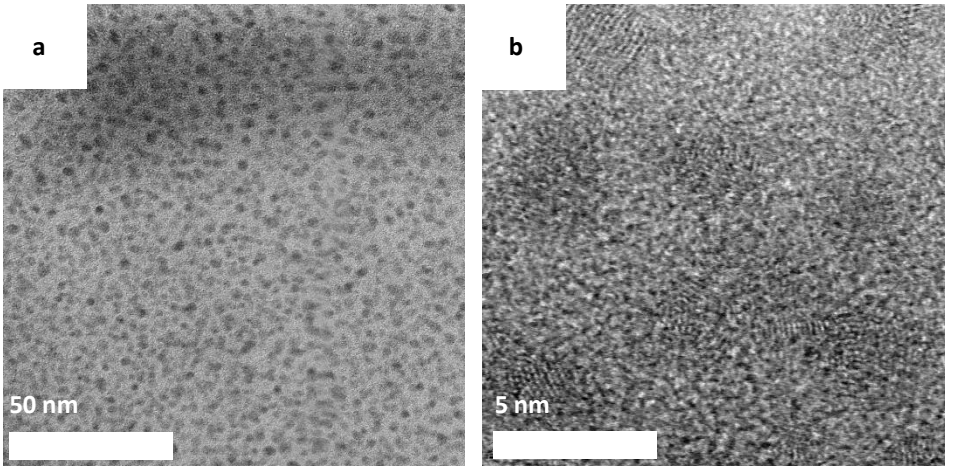

FIGURE 10.13
HR-TEM images of the synthesized GQDs by PLS using silver as a catalyst. (a)The image show the high density of the synthesized GQDs and the narrow size range; (b) the image show that the size range of the synthesized GQDs is 1-3 nm across

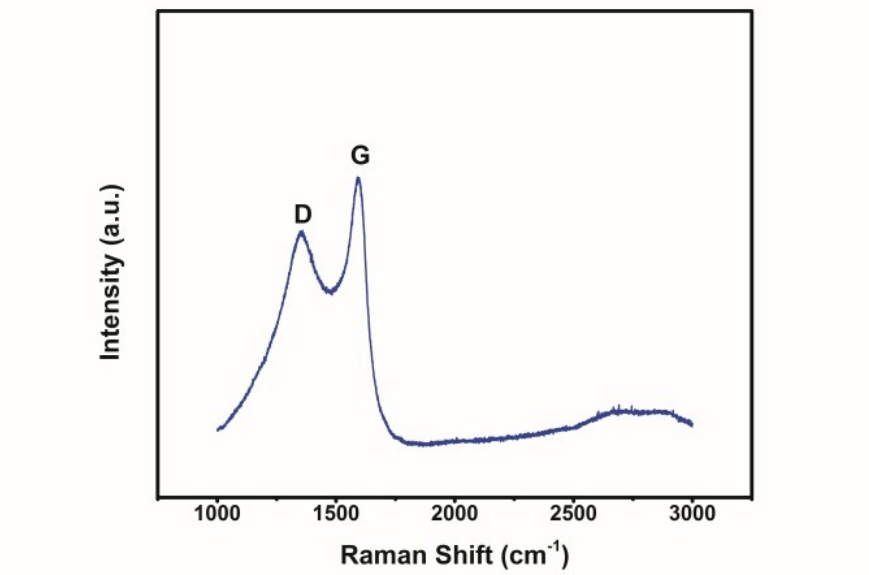

FIGURE 10.14
Raman spectrum of graphene nanostructures synthesized by the irradiation of the benzene-silver colloidal showing the D-band at 1353 cm^{-1}, G-band at 1593 cm^{-1}, and 2D band centered around 2660 cm^{-1}, the spectrum is consistent with the spectrum of GQDs (see Fig. 10.9)

Summary

An overview of pulsed laser synthesis techniques applied to the fabrication of nanoparticles, has been presented and the concepts of bottom-up and the top-down synthesis within the description of each methodology in PLS are described. Experimental setups for the synthesis of nanostructures using PLS were discussed, showing its excellent suitability for the synthesis of a wide range of nanoparticles in terms of the yield and size homogeneity. We also discussed the synthesis of specific nanostructures by PLS, primarily focusing on the array of carbon-based nanostructures that can be obtained by changing the PLS conditions and parameters. In particular, the high-yield synthesis and comprehensive characterization of GQDs were discussed in detail. The synthesis mechanism was proposed for the formation graphene nanostructures, which is consistent with their composition and nanostructure as revealed by electron microscopy and spectroscopic techniques.

Acknowledgments

This research was carried out under the auspices of the Institute for Functional Nanomaterials (NSF Cooperative Agreement 1002410), PR NASA EPSCoR (NASA Cooperative Agreement NNX13AB22A), PR DOE EPSCoR (DOE Grant DE-FG02-08ER46526) and UPR GK-12 Fellowship Program (NSF Grant No. 0841338). We want to acknowledge Dr. M. Guinel for providing access to the Nanoscopy Facility and Mr. Oscar Resto taking the HR-TEM images.

References

1. Niewold P, Ann L, Manciu FS, Torres B, Alvarado M, Chianelli RR. Organic/inorganic complex pigments: Ancient colors Maya Blue. Journal of Inorganic Biochemistry 2007; 101(11- 12) 1958-973.
2. Freestone I, Meeks N, Sax M, Higgitt C. The Lycurgus Cup — A Roman nanotechnology. Gold Bulletin 2007; 40(4) 270-77.
3. Johnson-mcdaniel D, Barrett CA, Sharafi A, Salguero Tt. Nanoscience of an Ancient Pigment, Journal of American Chemical Society 2013; 135(5) 1677–1679.
4. Maiman TH. Stimulated Optical Radiation in Ruby. Nature 1960; 187 493-94.
5. Shirk MD, Molian PA. A review of ultrashort pulsed laser ablation of materials. Journal of Laser Applications 1998; 10(1) 18-28.
6. Yang GW. Laser ablation in liquids: Applications in the synthesis of nanocrystals. Progress in Materials Science 2007; 52 (4) 648-98.
7. Zeng H, Du X-W, Singh SC, Kulinich SA, Yang S, He J, Cai W. Nanomaterials via Laser Ablation/Irradiation in Liquid: A Review. Advanced Functional Material 2012; 22(7) 1333-1353.
8. Bäuerle D. Thermal, Photophysical, and Photochemical Processes. In: Laser Processing and Chemistry: Springer Berlin Heidelberg; 1996. p. 13-38.
9. Brown M.S., Arnold C.B. Fundamentals of Laser-Material Interaction and Application to Multiscale Surface Modification. In: Sugioka K., Meunier M., PiqueA (ed.) Laser Precision Microfabrication. Springer Series in Materials Science: Springer Berlin Heidelberg; 2010. p. 91-120.

10. Urech L., Lippert T. Photoablation of Polymer Materials, in Photochemistry and Photophysics of Polymer Materials. In: Allen N.S. (ed.) Photochemistry and Photophysics of Polymer Materials. Hoboken, NJ, USA: John Wiley & Sons, Inc.; 2010. Available from http://onlinelibrary.wiley.com/ (accessed 20 January 2014).
11. Bulgakova NM, Bulgakov AV. Pulsed laser ablation of solids: Transition from normal vaporization to phase explosion. Applied Physics A Materials Science & Processing 2001; 73 (2) 199-208.
12. Stoian R, Ashkenasi D, Rosenfeld A, Campbell EEB. Coulomb explosion in ultrashort pulsed laser ablation of Al2O3. Physical Review B 2000; 62 (19) 13167-13173.
13. Yoshino K, Fujii H, Inuishi Y. Influence of liquid hydrocarbon layer on laser-induced surface damage. Journal of Physics D: Applied Physics. 1978; 11(9) L127.
14. Manish P, Conforti PF, Garrison BJ. On the role of chemical reactions in initiating ultraviolet laser ablation in poly(methyl methacrylate). Journal of Applied Physics 2007; 101 (10) 103113.
15. Luk'yanchuk B, Bityurin N, Anisimov S, Malyshev A, Arnold N, Bäuerle D. Photophysical ablation of organic polymers: The influence of stresses. Applied Surface Science 1996; 106 120-25.
16. Iqbal P., Preece J.A., Mendes P.M. Nanotechnology: The ―Top-Down‖ and ―Bottom-Up‖ Approaches. In: Gale P., Steed J. (ed.) Supramolecular Chemistry: Hoboken, NJ, USA: John Wiley & Sons, Ltd; 2012. Available from http://onlinelibrary.wiley.com/ (accessed 25 February 2014).
17. Luther W (ed.). Industrial application of nanomaterials: chances and risks (Technological Analysis). Dusseldorf, Germany: Future Technologies of VDI Technologiezentrum GmbH; 2004, 54:1-112.
Available from: www.nanowerk.com/nanotechnology/reports/reportpdf/report27.pdf (accessed 28 February 2014).
18. Patra A, Métivier R, Piard J, Nakatani K. SHG-active molecular nanorods with intermediate photochromic properties compared to solution and bulk solid states. Chemical Communications 2010; 46 (34) 6385-6387.
19. Liu M. , Ji Z., Shang L. Part One Top-Down Strategy: Top-Down Fabrication of Nanostructures. In: Chi L. (ed.) Nanotechnology: Volume 8: Nanostructured Surfaces: Weinheim, Germany WILEY-VCH Verlag GmbH & Co.; 2010. p. 1- 48 Available from: http://www.wiley-vch.de/books/sample/3527317392_c01.pdf (accessed 3 March 2014).
20. Brent A.R., Dong Q. Nanotechnology: A Top-Down Approach. Encyclopedia of Supramolecular Chemistry. UK: Taylor & Francis; 2007. p. 1-9. Available from: http://www.tandfonline.com/doi/abs/10.1081/E-ESMC-120047104#.U0WDoPldUSO (accessed 10 March 2014).
21. Bondi SN, Lackey WJ, Johnson RW, Wang X, Wang ZL. Laser assisted chemical vapor deposition synthesis of carbon nanotubes and their characterization. Carbon 2006; 44 1393-403.
22. Chen C, Chen W, Zhang Y. Synthesis of carbon nano-tubes by pulsed laser ablation at normal pressure in metal nano-sol. Physica E: Low-dimensional Systems and Nanostructures 2005; 28 (2) 121-27.
23. Fukata N, Oshima T, Tsurui T, Ito S, Murakami K. Synthesis of silicon nanowires using laser ablation method and their manipulation by electron beam. Science and Technology of Advanced Materials 2005; 6 (6) 628-32.
24. Prashant K, Panchakarla LS, Rao CNR. Laser-induced unzipping of carbon nanotubes to yield graphene nanoribbons. Nanoscale 2011; 3 (5) 2127-2129.

25. Russo P, Hu A, Compagnini G, Duley WW, Zhou NY. Femtosecond laser ablation of highly oriented pyrolytic graphite: A green route for large-scale production of porous graphene and graphene quantum dots. Nanoscale 2014; 6 (4) 2381-2389.
26. Anikin KV, Melnik NN, Simakin AV, Shafeev GA, Voronov VV, Vitukhnovsky AG. Formation of ZnSe and CdS quantum dots via laser ablation in liquids. Chemical Physics Letters 2002; 366 (3-4) 357-360.
27. Semaltianos N, Logothetidis S, Perrie W, Romani S, Potter R, Sharp M, French P, Dearden G, Watkins K. CdSe nanoparticles synthesized by laser ablation. EPL (Europhysics Letters) 2008; 84 (4) 47001.
28. Wesolowski MJ, Kuzmin S, Wales B, Sanderson JH, Duley WW. Self-assembly of thin carbon micro-shells through pulsed laser irradiation of a ferrocene/benzene solution. Journal of Materials Science 2013; 48 (18) 6212-6217.
29. Patil P, Phase D, Kulkarni S, Ghaisas S, Kulkarni S, Kanetkar S, Ogale S, Bhide V. Pulsed- laser–induced reactive quenching at liquid-solid interface: Aqueous oxidation of iron. Physical Review Letters 1987; 58 (3) 238-241.
30. Smith MJ, Sher M-J, Franta B, Lin Y-T, Mazur E, Gradečak S. Improving dopant incorporation during femtosecond-laser doping of Si with a Se thin-film dopant precursor. Applied Physics A 2014; 114 (4) 1009-1016.
31. Geohegan DB, Puretzky AA, Duscher G, Pennycook SJ. Time-resolved imaging of gas phase nanoparticle synthesis by laser ablation. Applied Physics Letters 1998; 72 (23) 2987-2989.
32. Hussein AE, Diwakar PK, Harilal SS, Hassanein A. The role of laser wavelength on plasma generation and expansion of ablation plumes in air. Journal of Applied Physics 2013; 113 (14) 143305.
33. Pola J, Urbanová M, Bastl Z, Plzák Z, Šubrt J, Vorlíček V, Gregora I, Crowley C, Taylor R. Laser photolysis of liquid benzene and toluene: Graphitic and polymeric carbon formation at ambient temperature. Carbon 1997; 35 (5) 605-611.
34. Scott CD, Arepalli S, Nikolaev P, Smalley RE. Growth mechanisms for single-wall carbon nanotubes in a laser-ablation process. Applied Physics A Materials Science & Processing 2001; 72 (5) 573-580.
35. Li Yang L. Self-Assembly and Ordering Nanomaterials by Liquid-Phase Pulsed Laser Ablation. PhD thesis. University of Bristol; 2007.
36. Llamas-Jansa I, Jäger C, Mutschke H, Henning TH. Far-ultraviolet to near-infrared optical properties of carbon nanoparticles produced by pulsed-laser pyrolysis of hydrocarbons and their relation with structural variations. Carbon 2007; 45 (7) 1542-1557.
37. Mordkovich VZ. The Observation of Large Concentric Shell Fullerenes and Fullerene-like Nanoparticles in Laser Pyrolysis Carbon Blacks. Chemistry of Materials 2000; 12 (9) 2813-2818.
38. Cauchetier M, Armand X, Herlin N, Alexandrescu R, Morjan I, Petcu S, Voicu I. Laser Pyrolysis of Hydrocarbons in Synthesis of Soot Containing Fullerenes. Fullerene Science and Technology 1999; 7 (1) 91-110.
39. Toyota K, Nakashima S, Okada T. Near-infrared laser-induced breakdown of liquid benzene. Chemical Physics Letters 2000; 323 (3-4) 323-328.
40. Gokhale RR, Thakare VP, Warule S, Lefez B, Hannoyer B, Jog JP, Ogale SB. From small aromatic molecules to functional nanostructured carbon by pulsed laser-induced photochemical stitching. AIP Advances 2012; 2 (2) 022130.

41. Gokhale R, Singh P. Blue Luminescent Graphene Quantum Dots by Photochemical Stitching of Small Aromatic Molecules: Fluorescent Nanoprobes in Cellular Imaging. Particle & Particle Systems Characterization 2014; 31 (4) 433-438.
42. Nkosi SS, Mwakikunga BW, Sideras-Haddad E, Forbes A. Synthesis and characterization of potential iron–platinum drugs and supplements by laser liquid photolysis. Nanotechnology, Science and Applications 2012; 2012:5 27-36.
43. Kim CH, Im HS, Cho YJ, Jung CS, Jang DM, Myung Y, et al. High-Yield Gas-Phase Laser Photolysis Synthesis of Germanium Nanocrystals for High-Performance Photodetectors and Lithium Ion Batteries. The Journal of Physical Chemistry C. 2012; 116(50):26190-6.
44. Watanabe M, Takamura H, Sugai H. Preparation of Ultrafine Fe–Pt Alloy and Au Nanoparticle Colloids by KrF Excimer Laser Solution Photolysis. Nanoscale Research Letters 2009; 4 (6) 565-573.
45. Christen H, Eres G. Recent advances in pulsed-laser deposition of complex oxides. Journal of Physics: Condensed Matter 2008; 20 (26) 264005.
46. Mukaida M, Miura M, Ichinose A, Matsumoto K, Yoshida Y, Horii S, Saito A, Hirose F, Takahashi Y, Ohshima S. Hetero-Epitaxial Growth of CeO Films on MgO Substrates. Japanese Journal of Applied Physics 2005; 44 L318-321.
47. Kim H, Horwitz JS, Kushto GP, Kafafi ZH, Chrisey DB. Indium tin oxide thin films grown on flexible plastic substrates by pulsed-laser deposition for organic light-emitting diodes. Applied Physics Letters 2001; 79 (3) 284.
48. Craciun V, Craciun D, Wang X, Anderson TJ, Singh RK. Highly conducting indium tin oxide films grown by ultraviolet-assisted pulsed laser deposition at low temperatures. Thin Solid Films 2004; 453-454 256-261.
49. Lin H, Rumaiz AK, Schulz M, Wang D, Rock R, Huang CP, Shah I. Photocatalytic activity of pulsed laser deposited TiO2 thin films. Materials Science and Engineering: B 2008; 151 (2) 133-139.
50. Chen J, Wang L, Su X, Kong L, Liu G, Zhang X. InGaZnO semiconductor thin film fabricated using pulsed laser deposition. Optics Express 2010; 18 (2) 1398.
51. Hidalgo A, Makarov V, Morell G, Weiner B. High-Yield Synthesis of Cubic and Hexagonal Boron Nitride Nanoparticles by Laser Chemical Vapor Decomposition of Borazine. Dataset Papers in Nanotechnology 2013; 2013 281672- 281676.
52. Sajjad M, Zhang H, Peng X, Feng P. Effect of substrate temperature in the synthesis of BN nanostructures. Physica Scripta 2011; 83 (6) 065601.
53. Sajjad M, Morell G, Feng P. Advance in Novel Boron Nitride Nanosheets to Nanoelectronic Device Applications. ACS Applied Materials & Interfaces 2013; 5 (11) 5051-5056.
54. Sajjad M, Feng P. Low temperature synthesis of c-BN films. Applied Physics Letters 2011; 99 (25) 253109.
55. Reisse G, Weissmantel S. Pulsed laser deposition of hexagonal and cubic boron nitride films. Applied Physics A: Materials Science & Processing 1999; 69 (1) S749-753.
56. Komatsu S, Shimizu Y, Moriyoshi Y, Okada K, Mitomo M. Preparation of boron nitride nanocapsules by plasma-assisted pulsed laser deposition. Journal of Applied Physics 2002; 91 (9) 6181.
57. Eason R. Pulsed Laser Deposition of Thin Films: Application-Led Growth of Functional Materials. Hoboken, New Jersey: John Wiley & Sons Inc.; 2007.
58. Chrisey DB, Hubler G.K. Pulsed Laser Deposition of Thin Films. Weinheim, Germany: WILEY-VCH Verlag GmbH & Co.; 1994.

59. Buzea C, Pacheco II, Robbie K. Nanomaterials and nanoparticles: Sources and toxicity. Biointerphases 2007; 2 (4) MR17-MR71.
60. Kelly KL, Lance E, Coronado L, Zhao LL, Schatz GC. The Optical Properties of Metal Nanoparticles: The Influence of Size, Shape, and Dielectric Environment. The Journal of Physical Chemistry B 2003; 107 (3) 668-677.
61. Mafuné F, Kohno J-Y, Takeda Y, Kondow T. Full Physical Preparation of Size-Selected Gold Nanoparticles in Solution: Laser Ablation and Laser-Induced Size Control. The Journal of Physical Chemistry B 2002; 106 (31) 7575-7577.
62. Amendola V, Polizzi S, Meneghetti M. Free Silver Nanoparticles Synthesized by Laser Ablation in Organic Solvents and Their Easy Functionalization. Langmuir 2007; 23 (12) 6766- 6770.
63. Morales AM, Lieber CM. A Laser Ablation Method for the Synthesis of Crystalline Semiconductor Nanowires. Science 1998; 279 (5348) 208-211.
64. Singh S.C., Zeng H., Guo C., Cai W. Nanomaterials: Processing and Characterization with Lasers, Weinheim, Germany: WILEY-VCH Verlag GmbH & Co.; 2012.
65. Almeida de Matos R, da Silva Cordeiro T, Elgul Samad R, Dias Vieira N, Jr., Coronato Courrol L. Green synthesis of gold nanoparticles of different sizes and shapes using agar–agar water solution and femtosecond pulse laser irradiation. Applied Physics A 2012; 109(3) 737-41.
66. Riabinina D, Zhang J, Chaker M, Margot J, Ma D. Size Control of Gold Nanoparticles Synthesized by Laser Ablation in Liquid Media. ISRN Nanotechnology 2012; 2012:5.
67. Sylvestre, J-P, Kabashin AV, Sacher E, Meunier M, Luong JHT. Stabilization and Size Control of Gold Nanoparticles during Laser Ablation in Aqueous Cyclodextrins. Journal of the American Chemical Society 2004; 126 (23) 7176-7177.
68. Tilaki RM., Zad AI, Mahdavi SM. Stability, size and optical properties of silver nanoparticles prepared by laser ablation in different carrier media. Applied Physics A 2006; 84 (1-2) 215-219.
69. Besner S, Kabashin AV, Winnik FM, Meunier M. Ultrafast laser based ―greenǁ synthesis of non-toxic nanoparticles in aqueous solutions. Applied Physics A 2008; 93 (4) 955-959.
70. Kubiliūtė R, Maximova KA, Lajevardipour A, Yong J, Hartley JS, Mohsin ASM, et al. Ultra- pure, water-dispersed Au nanoparticles produced by femtosecond laser ablation and fragmentation." International Journal of Nanomedicine 2013; 2013:8(1) 2601-611.
71. Sasaki T, Yoshiki Shimizu Y, Koshizaki N. Preparation of metal oxide-based nanomaterials using nanosecond pulsed laser ablation in liquids. Journal of Photochemistry and Photobiology A: Chemistry 2006; 182 (3) 335-341.
72. Salminen T, Dahl J, Tuominen M, Laukkanen P, Arola E, Tapio Niemi. Single-step fabrication of luminescent GaAs nanocrystals by pulsed laser ablation in liquids. Optical Materials Express 2012; 2 (6) 799.
73. Zhang J, Lan CQ. Nickel and cobalt nanoparticles produced by laser ablation of solids in organic solution. Materials Letters 2008; 62 (10-11) 1521-1524.
74. Semaltianos NG, Petkov P, Scholz S, Guetaz L. Palladium or palladium hydride nanoparticles synthesized by laser ablation of a bulk palladium target in liquids. Journal of Colloid and Interface Science 2013; 402 307-311.
75. Nath A, Laha SS, Khare A. Effect of focusing conditions on synthesis of titanium oxide nanoparticles via laser ablation in titanium–water interface. Applied Surface Science 2011; 257 (7) 3118-3122.
76. Compagnini G, Sinatra MG, Messina GC, Patanè G, Scalese S, Puglisi O. Monitoring the formation of inorganic fullerene-like MoS2 nanostructures by laser ablation in liquid environments. Applied Surface Science 2012; 258 (15) 5672-5676.

77. Satoshi N, Akaishi M, Sasaki T, Yamaoka S. Characterizations of several cubic phases directly transformed from the graphitic BC2N. Materials Science and Engineering: A 1996; 209 (1-2) 26-29.
78. Wentorf RH. Cubic Form of Boron Nitride. The Journal of Chemical Physics 1957; 26 (4) 956.
79. Widany J, Frauenheim Th, Köhler Th, Sternberg M, D. Porezag D, Jungnickel G, et al. Density-functional-based construction of transferable nonorthogonal tight-binding potentials for B, N, BN, BH, and NH. Physical Review B 1996; 53 (8) 4443-4452.
80. Xiong YH, Xiong CS, Wei SQ, Yang HW, Mai YT, XuW, et al. Study on the bonding state for carbon–boron nitrogen with different ball milling time. Applied Surface Science 2006; 253 (5) 2515-2521.
81. Knittle E, Wentzcovitch RM, Jeanloz R, Cohen ML. Experimental and theoretical equation of state of cubic boron nitride. Nature 1989; 337 (6205) 349-352.
82. Mirkarimi PB, Mccarty KF, Medlin DL. Review of advances in cubic boron nitride film synthesis. Materials Science and Engineering: R: Reports 1997; 21 (2) 47-100.
83. Song L, Ci L, Lu H, Sorokin PB, Jin C, Ni J, et al. Large Scale Growth and Characterization of Atomic Hexagonal Boron Nitride Layers. Nano Letters 2010; 10 (8) 3209-3215.
84. Reich S, Ferrari A, Arenal R, Loiseau A, Bello I, Robertson J. Resonant Raman scattering in cubic and hexagonal boron nitride. Physical Review B 2005; 71 (20) 205201.
85. Ugarov MV, Ageev VP, Konov VI. Chemical vapour deposition of boron nitride films stimulated by ultraviolet radiation pulses from a KrF excimer laser. Quantum Electronics 1995; 25 (7) 679-683.
86. Ugarov MV, Ageev VP, Karabutov AV. UV laser induced interfacial synthesis of CN-BCN layers on diamond films in borazine and ammonia. Applied Surface Science 1999; 138-139 (1– 4) 359–363.
87. Narita I, Oku T. Direct high-resolution electron microscopy of BN nanotubes with hexagonal zigzag network. Chemical Physics Letters 2003; 377(3-4) 354–358.
88. Wang J, Yap YK. Growth of adhesive cubic phase boron nitride films without argon ion bombardment. Diamond and Related Materials 2006; 15 (2-3) 444–447.
89. Geim AK, Novoselov KS. The rise of graphene. Nature Materials 2007; 6(3) 183–191.
90. Mann M., Milne B., Teo K. Engineering the Synthesis of Carbon Nanotubes to Fabricate Novel Nanostructures. In: Waqar A, Jackson M. (ed.) Emerging Nanotechnologies for Manufacturing. Oxford, U.K.: 2009. p131.
91. Zhang LL, Zhao XS. Carbon-based materials as supercapacitor electrodes. Chemical Society Reviews 2009; 38 (9) 2520-2531.
92. Cha C, Shin SR, Annabi N, Dokmeci MR, Khademhosseini A. Carbon-Based Nanomaterials: Multifunctional Materials for Biomedical Engineering. ACS Nano 2013; 7(4) 2891-2897.
93. Huang Y, Liang J, Chen Y. An Overview of the Applications of Graphene-Based Materials in Supercapacitors. Small 2012; 8(12) 1805–1834.
94. Novoselov KS, Fal'ko VI, Colombo L, Gellert PR, Schwab MG, Kim K. A roadmap for graphene. Nature 2012; 490 (7419) 192-200.
95. Choi W, Lahiri I, Seelaboyina R, Kang YS. Synthesis of Graphene and Its Applications: A Review. Critical Reviews in Solid State and Materials Sciences 2010; 35 (1) 52-71.
96. Coakley KM, McGehee MD. Conjugated Polymer Photovoltaic Cells. Chemistry of Materials 2004; 16(23) 4533-4542.
97. Sun S.-S. , Serdar N. Organic photovoltaics: Mechanism, materials, and devices. Boca Raton, FL: Taylor & Francis; 2005.

98. Soppimath KS, Aminabhavi TM, Kulkarni AR, Rudzinski WE. Biodegradable polymeric nanoparticles as drug delivery devices. Journal of Controlled Release 2001; 70 (1-2) 1-20.
99. Jayakumar R, Menon D, Manzoor K, Nair SV, Tamura H. Biomedical applications of chitin and chitosan based nanomaterials—A short review. Carbohydrate Polymers 2010; 82 (2) 227-232.
100. Vlerken LEV, Amiji MM. Multi-functional polymeric nanoparticles for tumour-targeted drug delivery. Expert Opinion on Drug Delivery 2006; 3 (2) 205-216.
101. Piazza F, Solá F, Resto O, Fonseca LF, Morell G. Synthesis of diamond nanocrystals on polyimide film. Diamond and Related Materials 2009; 18 (2-3) 113-116.
102. Mendoza F, Hernández DM, Makarov V, Febus E, Weiner BR, Morell G. Room temperature gas sensor based on tin dioxide-carbon nanotubes composite films. Sensors and Actuators B: Chemical 2014; 190 (2-3) 227-233.
103. Li X, Magnuson CW, Venugopal A, An J, Suk JW, Han B, et al. Graphene Films with Large Domain Size by a Two-Step Chemical Vapor Deposition Process. Nano Letters 2010; 10 (11) 4328-4334.
104. Varshney D, Sumant AV, Resto O, Mendoza F, Quintero KP, Ahmadi M, Weiner BR, Morell G. Single-step route to hierarchical flower-like carbon nanotube clusters decorated with ultrananocrystalline diamond. Carbon 2013; 63 253-262.
105. Zhang D, Yan T, Shi L, Peng Z, Wen X, and Zhang J. Enhanced capacitive deionization performance of graphene/carbon nanotube composites. Journal of Materials Chemistry 2012; 22 (29) 14696-14704.
106. Shawky A, Yasuda S, Murakoshi K. Room-temperature synthesis of single-wall carbon nanotubes by an electrochemical process. Carbon 2012; 50(11) 4184-4191.
107. Hwang CC, Jin Z, Lu W, Sun Z, Alemany LB, Lomeda JR, Tour JM. In situ Synthesis of Polymer-Modified Mesoporous Carbon CMK-3 Composites for CO2 Sequestration. ACS Applied Materials & Interfaces 2011; 3 (12) 4782-4786.
108. Habiba K, Makarov VI, Avalos J, Guinel MJF, Weiner BR, Morell G. Luminescent graphene quantum dots fabricated by pulsed laser synthesis. Carbon 2013; 64 341-350.
109. Schauerman CM, Alvarenga J, Landi BJ, Cress CD, Raffaelle RP. Impact of nanometal catalysts on the laser vaporization synthesis of single wall carbon nanotubes. Carbon 2009; 47 (10) 2431-2435.
110. Wakabayashi T, Saikawa M, Wada Y, Minematsu T. Isotope scrambling in the formation of cyanopolyynes by laser ablation of carbon particles in liquid acetonitrile. Carbon 2012; 50 (1) 47-56.
111. Hu S, Bai P, Tian F, Cao S, Sun J. Hydrophilic carbon onions synthesized by millisecond pulsed laser irradiation. Carbon 2009; 47 (3) 876-883.
112. Yang L, May PW, Yin L, Smith JA, Rosser KN. Growth of diamond nanocrystals by pulsed laser ablation of graphite in liquid. Diamond and Related Materials 2007; 16(4-7) 725-729.
113. Amans D, Chenus AC, Ledoux G, Dujardin C, Reynaud C, Sublemontier O, Karine Masenelli-Varlot, Guillois O. Nanodiamond synthesis by pulsed laser ablation in liquids. Diamond and Related Materials 2009; 18 (2-3) 177-180.
114. Liu P, Cao YL, Wang CX, Chen XY, Yang GW. Micro- and Nanocubes of Carbon with C8-like and Blue Luminescence. Nano Letters 2008; 8 (8) 2570-2575.
115. Sun YP, Zhou B, Lin Y, Wang W, Shiral Fernando KA, Pathak P, et al. Quantum-Sized Carbon Dots for Bright and Colorful Photoluminescence. Journal of the American Chemical Society 2006; 128 (24) 7756-7757.

116. Li X, Wang H, Shimizu Y, Pyatenko A, Kawaguchi K, Koshizaki N. Preparation of carbon quantum dots with tunable photoluminescence by rapid laser passivation in ordinary organic solvents. Chemical Communications 2010; 47 (3) 932-934.
117. Mortazavi SZ, Parvin P, Reyhani A. Fabrication of graphene based on Q-switched Nd:YAG laser ablation of graphite target in liquid nitrogen. Laser Physics Letters 2012; 9(7) 547-552.
118. Oyama T, Ishii T, Takeuchi K. Synthesis of Fullerenes by Ablation Using Pulsed and cw- Nd:YAG Lasers. Fullerene Science and Technology 1997; 5(5) 919-933.
119. Zhu S, Zhang J, Qiao C, Tang S, Li Y, Yuan W, et al. Strongly green-photoluminescent graphene quantum dots for bioimaging applications. Chemical Communications 2011; 47(24) 6858-6860.
120. Peng J, Gao W, Gupta BK, Liu Z, Romero-Aburto R, Ge L, et al. Graphene Quantum Dots Derived from Carbon Fibers. Nano Letters 2012; 12(2) 844-849.
121. Wang C, Wu C, Zhou X, Han T, Xin X, Wu J, et al. Enhancing Cell Nucleus Accumulation and DNA Cleavage Activity of Anti-Cancer Drug via Graphene Quantum Dots. Scientific Reports 2013; 3.
122. Markovic ZM, Ristic BZ, Arsikin KM, Klisic DG, Harhaji-Trajkovic LM, Todorovic-Markovic BM, et al. Graphene quantum dots as autophagy-inducing photodynamic agents. Biomaterials 2012; 33(29) 7084-7092.
123. Qu D, Zheng M, Du P, Zhou Y, Zhang L, Li D, et al. Highly luminescent S, N co-doped graphene quantum dots with broad visible absorption bands for visible light photocatalysts. Nanoscale 2013; 5 (24) 12272-12277.
124. Zhu Y, Zhao N, Lian J, Jiang Q. Toward Tandem Photovoltaic Devices Employing Nanoarray Graphene-Based Sheets. The Journal of Physical Chemistry C 2014; 118(5) 2385–2390.
125. Gupta V, Chaudhary N, Srivastava R, Sharma GD, Bhardwaj R, Chand S. Luminscent Graphene Quantum Dots for Organic Photovoltaic Devices. Journal of the American Chemical Society 2011; 133 (26) 9960-9963.
126. Mihalache I, Radoi A, Munteanu C, Kusko M, Kusko C. Charge storage and memory effect in graphene quantum dots – PEG600 hybrid nanocomposite. Organic Electronics 2014; 15 (1) 216-225.
127. Tang L, Ji R, Cao X, Lin J, Jiang H, Li X, et al. Deep Ultraviolet Photoluminescence of Water-Soluble Self-Passivated Graphene Quantum Dots. ACS Nano 2012; 6 (6) 5102-5110.
128. Lee J, Kim K, Park WI, Kim B-H, Park JH, Kim T-H, et al. Uniform Graphene Quantum Dots Patterned from Self-Assembled Silica Nanodots. Nano Letters 2012; 12(12) 6078-6083.
129. Park S, An J, Piner RD, Jung I, Yang D, Velamakanni A, Nguyen ST, Ruoff RS. Aqueous Suspension and Characterization of Chemically Modified Graphene Sheets. Chemistry of Materials 2008; 20(21) 6592-6594.
130. Yuan D, Chen J, Hu X, Zeng J, Tan S, Liu Y. Large-scale synthesis of monodispersed carbon microflakes for electric double-layer capacitors. International Journal of Electrochemical Science 2008; 3(11) 1268–1276.
131. Russo P, Hu A, Compagnini G. Synthesis, Properties and Potential Applications of Porous Graphene: A Review. Nano-Micro Letters 2013; 5 (4) 260-273.